Available online at www.sciencedirect.com
SCIENCE DIRECT®
International Journal of Mass Spectrometry 240 (2005) 301–315
International Journal of Mass Spectrometry
www.elsevier.com/locate/ijms

Ion mobility–mass spectrometry: a new paradigm for proteomics

John A. McLean, Brandon T. Ruotolo, Kent J. Gillig, David H. Russell*

Department of Chemistry, Laboratory for Biological Mass Spectrometry, Texas A&M University, 3255 TAMU, College Station, TX 77843, USA

Received 30 August 2004; accepted 1 October 2004
Available online 13 November 2004

Abstract

Matrix-assisted laser desorption/ionization (MALDI) coupled with ion mobility–mass spectrometry (IM–MS) provides a rapid (μs–ms) means for the two-dimensional (2D) separation of complex biological samples (e.g., peptides, oligonucleotides, glycoconjugates, lipids, etc.), elucidation of solvent-free secondary structural elements (e.g., helices, β-hairpins, random coils, etc.), rapid identification of post-translational modifications (e.g., phosphorylation, glycosylation, etc.) or ligation of small molecules, and simultaneous and comprehensive sequencing information of biopolymers. In IM–MS, protein-identification information is complemented by structural characterization data, which is difficult to obtain using conventional proteomic techniques. New avenues for enhancing the figures of merit (e.g., sensitivity, limits of detection, dynamic range, and analyte selectivity) and optimizing IM–MS experimental parameters are described in the context of deriving new information at the forefront of proteomics research.

Keywords: Ion mobility; Mass spectrometry; Ion mobility-mass spectrometry; Proteomics; Biopolymers

1. Contemporary proteomics by mass spectrometry and the ion mobility–mass spectrometry method

Advances in the field of proteomics parallel technological advances in mass spectrometry techniques for the purposes of protein separation, identification, and characterization [1]. Mass spectrometry-based protein identification has advanced rapidly over the past decade through the development of bottom–up MS [2] and top–down MS [3] techniques. Considerable developmental research is still focused on improving the sensitivity, dynamic range, information content, and data-interpretation algorithms in these types of experiments [4]. Recent developments in instrumentation for ion mobility spectrometry (IMS), a gas-phase post-ionization separation method, coupled with mass spectrometry (IM–MS) reveals potential applications of this relatively new technique for rapid, high-resolution separations of analytes based on structure (ion conformation) and mass-to-charge (*m*/*z*) ratios. Although IM–MS separations can be achieved at resolutions comparable to high-performance liquid chromatography (HPLC) and capillary electrophoresis (CE), most IM–MS instruments are operated at relatively low IM resolution to reduce analysis time, maximize sample throughput, and reduce the complexity of interfacing IM with MS [5–8].

Typical proteomic-scale questions require a large number of measurements (determination of molecular weight and amino acid sequence, screening for post-translational modifications, etc. [9]) and broad dynamic range (e.g., protein concentrations ranging from 1×10^{-3} to 1×10^{-24} mol L^{-1} for human plasma proteins [10]); therefore, such techniques must afford high throughput at low limits of detection, high sensitivity, and wide dynamic range. Mass spectrometry, especially time-of-flight MS (TOFMS), provides many such capabilities, but the fundamental challenge in developing proteomics IM–TOFMS instrumentation is that IMS suffers from poor sensitivity and limits of detection (nmol–pmol). This is attributed to several factors including poor ionization efficiency, reduced ion transmission into the IM drift cell, ion losses in the uniform electrostatic-field drift cell (by diffusion and scattering processes), and ion losses that occur between the differential aperture and the TOF source as

* Corresponding author. Tel.: +1 979 845 3345; fax: +1 979 845 9485.
E-mail address: russell@mail.chem.tamu.edu (D.H. Russell).

1387-3806/$ – see front matter © 2004 Elsevier B.V. All rights reserved.
doi:10.1016/j.ijms.2004.10.003

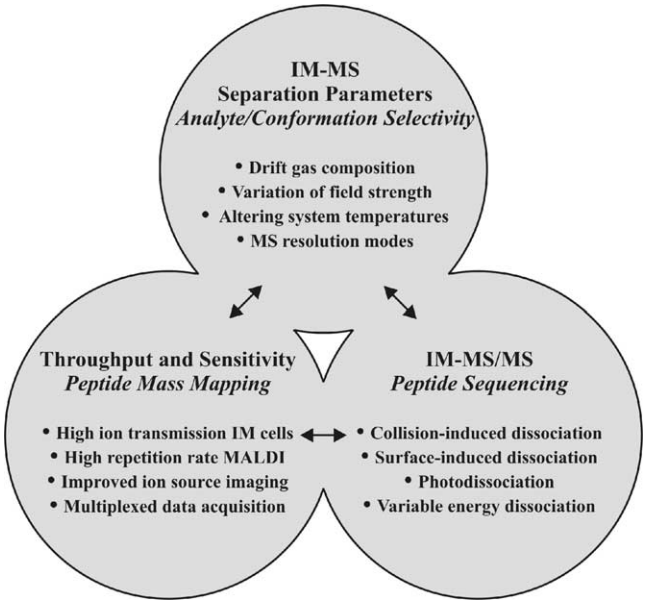

Fig. 1. Diagram illustrating the relationship between the three target areas for instrumental design efforts in IM for proteomic applications. Advances in each area complement or enhance the capabilities of each of the other target areas.

discussed below. Current instrumental advances are aimed at overcoming these challenges, and these efforts are motivated by the unique capabilities afforded by IM–MS and IM–MS/MS such as suppression or elimination of chemical noise, rapid (μs–ms) separation of complex biological mixtures, and nearly simultaneous biopolymer sequencing.

Instrument design efforts aimed at applications in proteomics are conceived within the context of often competing experimental objectives. For example, the overall ion transmission efficiency, and thus, sensitivity and limits of detection, of a mass spectrometer are often sacrificed to obtain narrower ion energy distributions or spatial positions for higher resolution measurements. To mitigate the effects of competing experimental goals, we have focused IM–MS instrument design on three complementary areas of peptide and protein analysis as illustrated in Fig. 1. Note that IM–MS separation parameters, throughput and sensitivity, and IM–MS/MS, are connected. Thus, advances in one of these areas often benefits the other two. For instance, an increased ability to disperse peptide ion signals in the ion mobility dimension facilitates parallel tandem mass spectrometry experiments on mobility-separated peptide ions.

Fig. 1 lists several experiments and instrument configurations used to address the three main areas of interest. Although most of the points listed in Fig. 1 have been discussed elsewhere, the topic of MS-resolution modes has received comparatively little attention [11]. Similar to the above discussion of balance between ion transmission (sensitivity) and mass spectral resolution, intentional lowering of the resolution of the mass measurement enhances limits of detection and sensitivity relative to high-resolution mass measurement experiments, because all of the analyte signal is contained in a single channel rather than being dispersed across the entire isotope cluster. For protein identification experiments, it is often desirable to observe a larger number of low-resolution peptide ion signals (or peptide fragment ion signals in a tandem mass spectrometry experiment), rather than a lower number of high-resolution peptide isotope cluster ion signals. However, mass measurement accuracy on peptide ion signals where the isotope cluster is not resolved, is limited to ∼50 ppm and may be insufficient for high confidence level protein identification [12]. In IM–MS peptide mass-mapping experiments (e.g., bottom–up MS), the resolutions of both the IM and MS dimensions are tailored to provide an optimal balance between sensitivity and resolution for high confidence level protein identification.

1.1. Liquid chromatography–mass spectrometry versus ion mobility–mass spectrometry

Separations of complex biological mixtures using combinations of liquid chromatography (e.g., HPLC, CE, etc.) coupled with MS detection have addressed several of the analytical challenges encountered in proteomics [13–15]. An important attribute of LC–MS is the ability to increase the dynamic range of the analysis by attenuating chemical noise/instrumental background [4]. However, coupling LC to MS imposes significant limitations on both experimental design and independent optimization of the LC and MS separation conditions. Further, there is a large disparity in the timescales of the two-analyte dispersive dimensions [16]. Although modern TOF mass analyzers can acquire data at very high rates (e.g., 4×10^4 to 5×10^4 spectra s^{-1}), liquid-phase separations can require minutes to hours, which limits sample throughput of LC–MS instrumentation [16]. In many proteomic applications, the chromatography dimension is used to decrease the complexity of the sample, i.e., to fractionate the analytes prior to MS analysis, which forms the basis for techniques such as multidimensional protein identification technology [17,18]. Seldom is the chromatographic dimension used to provide reliable qualitative descriptors of the analyte, e.g., to distinguish between background and analyte components or molecular type (peptide versus lipid versus surfactant, etc.). Recently, Smith and co-workers examined chromatographic retention time in combination with high mass measurement accuracy to identify proteins from their constituent tryptic peptides [19]. This approach relies on the combination of retention time and molecular mass to uniquely (or near-uniquely) identify an analyte within a sample having well-defined composition (i.e., a mixture of peptides), rather than the qualitative utility of the separation method. Examples of such LC–MS correlation analyses in proteomics are rare, but are fundamental to 2D liquid-phase separations such as polyacrylamide gel electrophoresis (PAGE).

In contrast, correlation analysis in 2D IM–MS provides unique advantages in proteomic research, which are outlined herein. A typical 2D IM–MS separation of a model tryptic

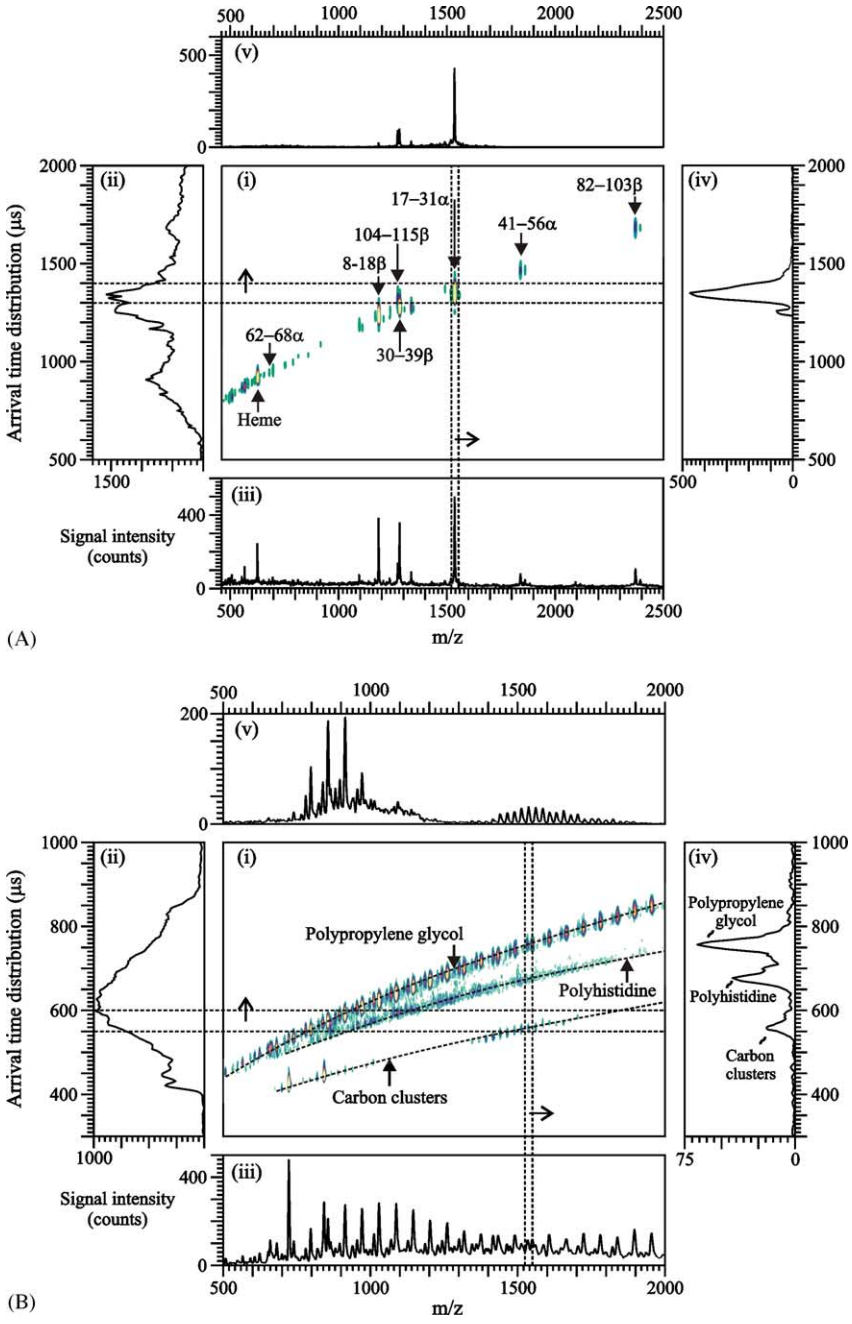

Fig. 2. (A): (i) Two-dimensional IM–MS plot of conformation space illustrating the separation of peptides obtained from a tryptic digest of bovine hemoglobin (adapted from Ref. [108]). (ii) The ion mobility ATD integrated over all *m*/*z* space. (iii) The mass spectrum obtained by integrating over all ATD space. (iv) The ATD integrated over the *m*/*z* range of 1525–1550 and (v) the mass spectrum obtained by integrating over the ATD of 1300–1400 μs (regions outlined by dashed lines). (B): (i) Two-dimensional IM–MS plot of conformation space showing the separation of a complex mixture of polypropylene glycol, polyhistidine, and carbon clusters (derived from C_{60}/C_{70}, which are used as both mass and mobility internal standards). (ii) The ion mobility ATD integrated over all *m*/*z* space. (iii) The mass spectrum obtained by integrating over all ATD space. (iv) The ATD integrated over the *m*/*z* range of 1525–1550 and (v) the mass spectrum obtained by integrating over the ATD of 550–600 μs (regions outlined by dashed lines). (C): (i) Two-dimensional IM–MS/MS plot of conformation space illustrating the separation of precursor peptides and their fragment ions from substance P, gramicidin S, bradykinin, and des[Arg^9]-bradykinin using SID ion activation (65 eV lab frame energy). (ii) The ion mobility ATD integrated over all *m*/*z* space. (iii) The mass spectrum obtained by integrating over all ATD space. (iv) The ATD integrated over the *m*/*z* range of 1025–1075 and (v) the mass spectrum obtained by integrating over the ATD of 950–975 μs (regions outlined by dashed lines). The drift cell was operated at 50 V cm^{-1} $Torr^{-1}$ with helium gas (A), 80 V cm^{-1} $Torr^{-1}$ with nitrogen gas (B), and 73 V cm^{-1} $Torr^{-1}$ with helium gas (C), respectively. MALDI was performed using α-cyano-4-hydroxycinnamic acid (CHCA) matrix with a frequency-tripled Nd:YAG laser (355 nm) operated at a repetition rate of 200 and 100 Hz in (A) and (B), respectively, and using a nitrogen laser (337 nm) operated at 30 Hz in (C).

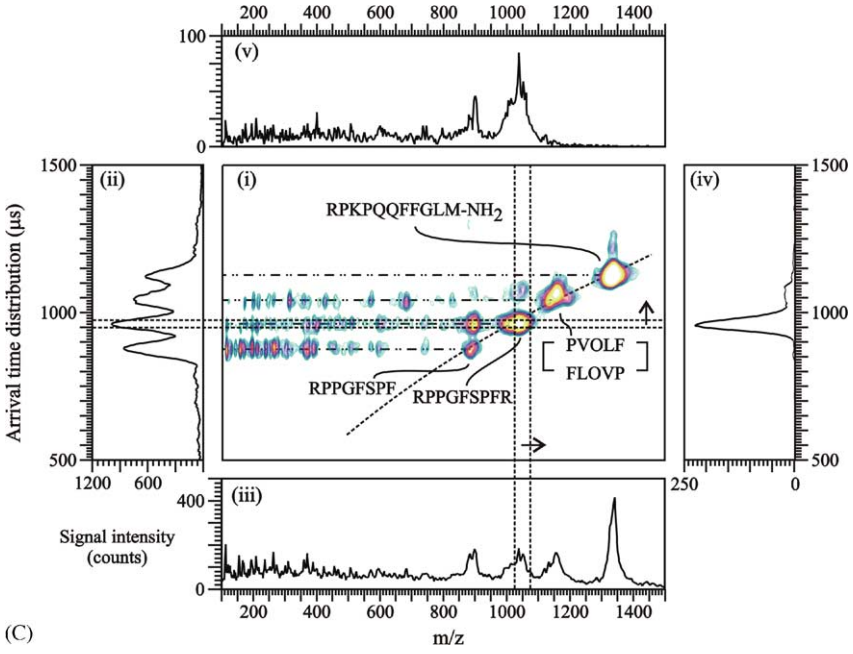

Fig. 2. (*Continued*).

digest is shown in Fig. 2(A) and emphasizes the advantages of IM–MS over mass spectrometry alone. Fig. 2(B) shows the separation of a complex mixture of polypropylene glycol (a model surfactant), polyhistidine (a model distribution of peptides), and carbon clusters (derived from fullerenes (C_{60}/C_{70}) used as internal calibrants). The mass spectrum obtained for this sample is shown in the bottom panel (Fig. 2(B, iii)), and the IM arrival time distribution (ATD) obtained without MS is contained in the left panel (Fig. 2(B, ii)). By coupling the two separation dimensions, a plot of the IM–MS conformation space is obtained (Fig. 2(B, i)). A cursory examination of the "conformation space" data suggests the presence of multiple chemical constituents as the gas-phase ions from the three molecular classes exhibit different trends in ATD as a function of their *m*/*z* ratio (hereafter referred to as "trendlines").[1] The three distinct trendlines for the data shown in Fig. 2(B) illustrate relationships for gas-phase packing efficiency (carbon clusters > peptides > surfactant) and thus, appear in different regions of conformation space. Fig. 2(B) also illustrates the reduction in chemical noise, which can be particularly problematic in the analysis of complex biological samples. By integrating the ATD obtained over a narrow *m*/*z* range (1525–1550 Da in Fig. 2(B)), an ATD is obtained as in Fig. 2(B, iv), which closely resembles chromatograms of liquid-phase separation techniques. Note that baseline separation is achieved for analytes corresponding to nearly the same *m*/*z*, which would be challenging (if possible) to assign by MS techniques alone. Chemical suppression is reduced as illustrated in Fig. 2(B, v) where the mass spectrum is integrated over a narrow range of ATD space as indicated by the attenuated baseline and a reduced number of ion signals.

The primary advantages of IM separation over conventional liquid-phase separation techniques are two-fold: (i) significant reduction of separation times (μs–ms) commensurate with the timescale of the MS dimension (esp. TOFMS) and (ii) post-ionization separation provides information on the products of ionization rather than both neutral and ionic species. However, the two most serious challenges of IM–MS technology are poor sensitivity and limited peak capacity (ϕ) relative to alternative multidimensional separation approaches [34]. For example, Table 1 lists estimated peak capacities for a variety of separations and multidimensional methodology. Although the peak capacity for MALDI–IM–MS is somewhat lower than that of other techniques, the strength of the technique is its superior peak capacity production rate ($\phi\,s^{-1}$, ca. 3×10^6), which is due to the speed of the two separations. Although the strength of LC–MS strategies lies in the orthogonality of the two separation dimensions [43], IM–MS relies on the correlation between the two separation dimensions for different chemical classes (e.g., peptides, PTM peptides, DNA, lipids, etc.) [44,45] or conformational classes (e.g., α-helix, β-sheet, and random coil) [25], adding a dimension of information not

[1] The terminology we use to describe 2D separation space in IM–MS depends on the physical characteristics of the analyte that gives rise to separation selectivity. Listed here are three examples: (i) separation of geometric isomers (e.g., distonic versus conventional radical cations or enol-keto isomers of small organic ions [20], chiral isomers [21], *cis–trans* isomers [22], etc.), (ii) electronic state isomers of atomic and molecular ions (e.g., Kr^{2+} ($^1S_0$, $^3P_0$, $^3P_1$, $^3P_2$, and $^1D_2$) in Kr [20]), and (iii) conformational isomers of biopolymers (e.g., peptide/protein secondary structure [23–25], intramolecular charge solvation [26–29], small molecule–peptide ligation, or non-covalent complexes [30–33]). We term the two-dimensional IM–MS separation space encompassed in such systems as (i) geometric space, (ii) electronic state space, and (iii) conformation space, respectively.

Table 1
A comparison of the peak capacity (ϕ) and peak capacity production rate ($\phi\,s^{-1}$) of several dimensional separation methodologies[a]

Separation dimensions	Peak capacity (ϕ)	Peak capacity production rate ($\phi\,s^{-1}$)	Reference
One dimension			
Capillary electrophoresis (CE)[b]	1×10^3	0.5	
High-performance liquid chromatography (HPLC)[b]	60	0.03	
Ultrahigh pressure HPLC	3×10^2	0.2	[35]
Gas chromatography (GC)	75	6	[36]
Two dimensions			
2D-Polyacrylamide gel electrophoresis (PAGE)	1×10^4	0.3	[37]
HPLC–Capillary zone electrophoresis (CZE)	6.5×10^2	4	[38]
Capillary isoelectric focusing (CIEF)–MS/MS	9×10^2	0.3	[37]
LC–Fourier transform ion cyclotron resonance–MS	6×10^7	1.25×10^4	[39]
MALDI–ion mobility–TOFMS	5.5×10^3	2.8×10^6	[40]
Three dimensions			
HPLC-ion mobility–MS	4×10^5	1.2×10^2	[41]
Size exclusion chromatography–HPLC–CZE	2.8×10^3	0.2	[42]

[a] Representative values for the separation dimensions listed.
[b] Estimated from typical experimental conditions.

present in conventional liquid-phase separations. The observed signal correlations for a given class of molecules can also increase the confidence level for assignment of low-intensity signals, thus increasing dynamic range [46]. In the following sections, the design considerations, operational principles, and experimental constructs are briefly described for IM–MS and IM–MS/MS with a particular emphasis on the unique information that can be derived to facilitate proteomic research.

1.2. Instrumentation for MALDI–ion mobility–TOFMS

The type and dimensionality of data that are desired from an experiment dictates the ultimate design for IM–MS instrumentation. Three general types of IM–MS experiments for proteomic applications are illustrated in Fig. 2(A) peptide mass mapping for protein identification, (B) separation of analyte classes in conformation space, and (C) peptide/protein sequence confirmation or de novo sequencing. Although the data in Fig. 2 appear to be 2D, it is important to note that conformation space allows for further correlated experiments to be designed. For example, Fig. 2(C) illustrates IM–MS/MS, whereby the parent ions are activated for dissociation as they elute from the drift cell, but prior to being sampled by TOFMS. Because the fragment ions are sampled at the same drift time as the precursor ions, they are correlated in terms of ATD [8,47–49]. Recently, several laboratories have investigated variable temperature IM for enhanced resolution and the investigation of solvation processes [20,50–54]. The novel utility of variable temperature IM is demonstrated by the capacity to observe annealing of peptide or protein structures at elevated or reduced temperatures, permitting the elucidation of kinetic and thermodynamic parameters. This enhanced dimensionality provides great utility for studies at the forefront of biophysics [55–57], and as illustrated below, such measurement capabilities may prove beneficial for structural biology, i.e., studies of post-translational modifications and quaternary structure.

The primary focus of conventional proteomics research is protein identification. Importantly, IM–MS provides added dimensionality to protein identification in the form of structural information. In the pursuit of comprehensive systems biology [58], it is imperative to increase our understanding of structural biology and structure-function relationships. In the mid-1990s, Bowers and colleagues demonstrated the use of IM–MS for the determination of gas-phase peptide structure [26,59]. In a series of excellent studies, Jarrold and coworkers have investigated the helical propensity of model peptides [23,53,60–66] and sequential solvation of helical and compact globular systems [67–73]. Russell and Ruotolo studied conserved secondary structure elements in proteolytically derived (tryptic) peptides by MALDI–IM–MS [24,25]. Jarrold and Clemmer also described protein tertiary structure dependence on charge-state for model systems using electrospray ionization (ESI)–IM–MS [74–76], and Clemmer has investigated charge-state and temporally resolved folding transitions in protein tertiary structure [77–80]. More recently, Bowers has applied IM–MS to the study of protein misfolding/protein conformational diseases such as Alzheimer's disease [56], Parkinson's disease [57], or prion diseases (e.g., transmissible spongiform encephalopathies [81–83]). In these investigations, ESI–IM–MS was used to study two alloforms of the amyloid-β protein where Aβ42 is strongly linked with Alzheimer's disease (possibly due to enhanced rates of fibrillization and plaque formation [84]) and recently, the protein α-synuclein, which is implicated in Parkinson's disease [57]. Although biophysical information is readily accessible in IM–MS measurements, the instrumental description presented here is focused on the utility of IM–MS for rapid and high throughput proteomic applications.

MALDI [85,86] and ESI [87] are both effective for producing biomolecular ions for IM–MS [88–92]. However, due

to differences in the types of ions formed and ionization efficiency, the source selected will depend on the aim of the experiment. The designs presented here utilize MALDI as the ionization source for peptides and proteins rather than ESI and therefore differ from the majority of other IM–MS instrument platforms described in the literature [52,53,93–95]. Our choice of MALDI is based-on four considerations. First, MALDI produces predominantly singly charged ions, which increase sensitivity and reduces spectral congestion by not partitioning ions into several charge-state channels. Second, MALDI is an inherently pulsed source of ions defining t_0 for both time-dispersive separation dimensions (IM and TOFMS). Third, MALDI produces ions in both a temporally- (ns–ps) and spatially focused region (μm^2). Under these conditions, resolution is not limited by temporally gating the ion injection [54,96–98], and ion transmission efficiency is enhanced by better projection of the ion source onto the aperture plate defining the end of the drift cell analogous to ion projection in sector-field instrumentation [99]. Finally, MALDI is relatively tolerant to detergents and salts commonly used in biochemistry. One criticism of MALDI is that potentially time consuming and contaminating sample preparation procedures are often necessary, but these concerns are mitigated by the recent availability of robotic sample handling systems, which can be used to construct "proteomics analyzers" of virtually complete automation replete with sample archiving capabilities [100].

Complementary to high-throughput proteomic studies, most IM–MS instrument platforms are devoted to projects investigating gas-phase ion structure and utilize ESI sources. This preference for ESI over MALDI for studies of gas-phase structure is due to the perception that ESI produces gas-phase ions having three-dimensional structures that are representative of the solution-phase forces that act on the molecule prior to desolvation/ionization [101]. Although this supposition is based on a relatively small number of critical studies on conformations of ESI formed peptide and protein ions, there are even fewer examples of studies on the conformations of MALDI-formed ions [102]. There are, however, many similarities between crystal growth conditions in protein crystallography (the standard method of determining protein structures) and the solution conditions utilized in MALDI sample deposition. Further studies on the structures of peptide/protein ions and how solvents influence the MALDI ionization are currently underway in our laboratory.

A schematic diagram of the general features of MALDI–IM–TOFMS instrumentation developed in our laboratory is presented in Fig. 3(A). Briefly, MALDI ions are formed at the entrance aperture of the IM drift cell that is typically operated at 1–10 Torr of background gas (e.g., He, N_2, CH_4, Ar, etc.). The ion beam then passes through a differentially pumped TOFMS interface region and subsequently sampled in the source of a two-stage reflectron orthogonal TOFMS. This design was chosen to combine the elements of simplicity, ease-of-use, and high ion transport efficiency. To further enhance the ion transport efficiency through the drift cell, we use a so-called "periodic-focusing" drift cell design [103]. These drift cells are analogous to dc-only ion guides whereby radial diffusion of the ions is limited. By confining the ion beam to the central axis of the drift cell, ion transport efficiency can be increased by factors of ca. 10–1000 over uniform electrostatic field designs without a concomitant degradation in IM resolving power (i.e., the ion guide superimposes a small confining field on a large uniform electrostatic field).

An important aspect of the IM–MS experiment is the treatment of 2D data acquisition. The typical timescale for IM drift times range from ca. 500 to 2000 μs, while the flight time of ions in the TOFMS range from ca. 5 to 40 μs. Sequentially initiating TOFMS at a rate of 25–200 kHz and subsequently stitching the spectra to construct a composite plot of conformation space would limit the time resolution in the IM dimension to the sampling rate of the TOFMS. For example, in order to achieve the necessary TOF sampling frequency (8–10 TOFMS spectra per IM peak) for a typical IM elution profile (25–75 μs wide at baseline), the TOF sampling frequency would range up to 400 kHz and result in poor sampling efficiency for analytes exhibiting either high IM resolution or fast IM drift times. Thus, real-time sampling of all IM elution profiles would require flight times in the mass analyzer of a few microseconds (e.g., 2.5 μs at 400 kHz) to retain time correlation. This constraint is incompatible with conventional high-resolution TOFMS [104].

To overcome this challenge and decouple the time resolution in both separation dimensions, a time interleaving data acquisition scheme was developed [105]. This concept is illustrated in Fig. 3(B) whereby a series of interleaved TOFMS acquisition sequences are sequentially offset from the initial ionization laser pulse (t_0^{IM}) and recombined to generate a plot of conformation space. For example, as shown in Fig. 3(B), the first TOF acquisition sequence (interleave #1) is initiated at t_0^{IM} and contains 2000 TOF mass spectra each of 25 μs. For each successive laser pulse (t_0^{IM}), the initial TOFMS extraction (t_0^{TOF}) is offset by an amount equal to the desired time resolution in the IM dimension. For the case illustrated in Fig. 3(B), the desired IM time resolution is 2.5 μs, so each successive t_0^{TOF} is offset from the previous laser pulse by an increment of 2.5 μs (i.e., t_0^{TOF} interleave #2 = t_0^{IM} + 2.5 μs, t_0^{TOF} interleave #3 = t_0^{IM} + 5 μs, etc.). For a TOFMS extraction frequency of 40 kHz (one extraction every 25 μs), the sequence illustrated in Fig. 3(B) is completed in 10 interleaves, at which point the acquisition program returns to the non-delayed sequence ($t_0^{TOF} = t_0^{IM}$) and iterates until a desired level of signal averaging in conformation space is achieved. Although this approach adds a limited amount of scanning to IM–TOFMS data acquisition (ideally a non-scanning technology), the primary advantage of this method is the ability to independently define time resolution in both separation dimensions.

It is also important to recognize that parallel advances in contemporary TOFMS are readily transferred to IM–TOFMS

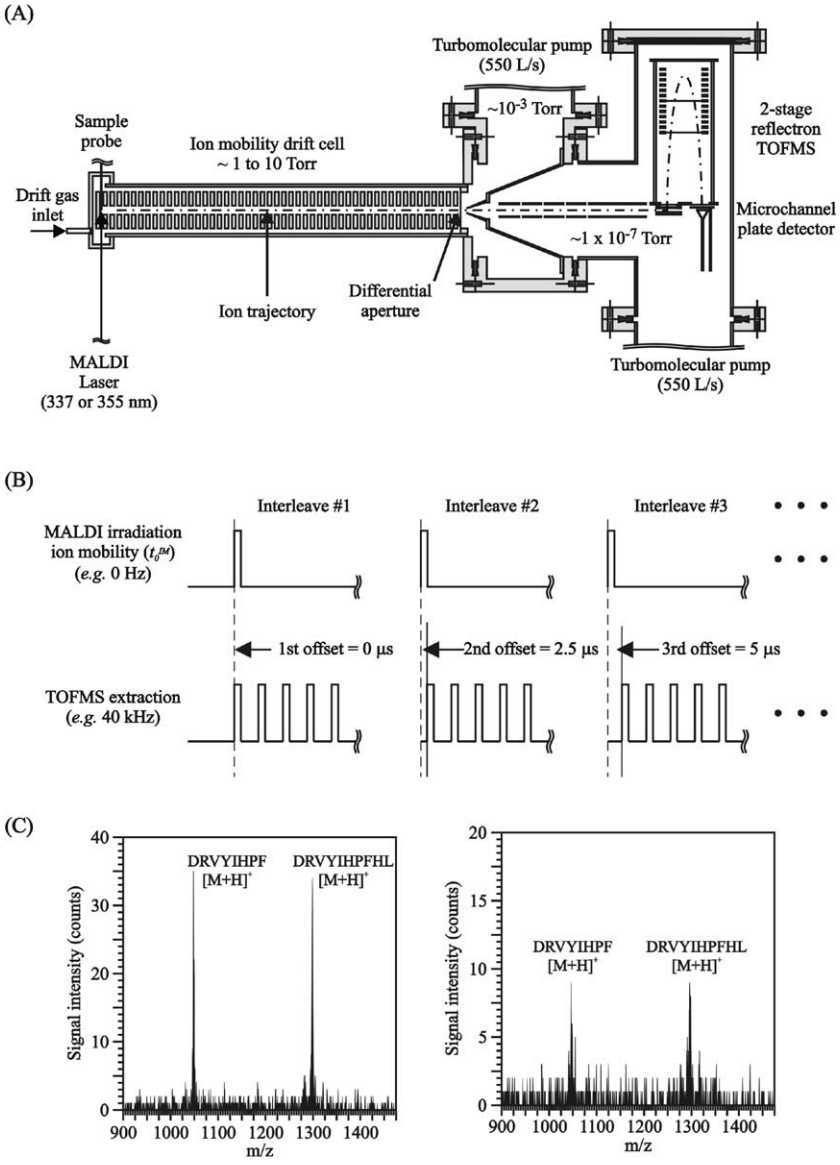

Fig. 3. (A) Schematic diagram of the MALDI–IM–TOFMS arrangement typically used in our laboratories. (B) Timing sequence diagram illustrating the interleaved data acquisition methodology used to independently define time resolution in the IM dimension, which is achieved by varying the interleave time offset and number of interleaves. Subsequently, all interleaves are stitched together to provide 2D IM–MS plots of conformation space (adapted from reference [105]). (C) (left) Integrated mass spectra over all ATD space of a mixture of 1.2 fmol human angiotensin II (DRVYIHPF, M_r = 1045.54 Da) and 0.96 fmol human angiotensin I (DRVYIHPFHL, M_r = 1295.69 Da) as deposited on the MALDI target. MALDI was performed using a frequency-tripled Nd:YAG laser (355 nm) at a laser repetition rate of 150 Hz. (B) Integrated mass spectrum of a mixture of 30 fmol angiotensin II and 24 fmol angiotensin I deposited on the MALDI target. MALDI was performed using a nitrogen laser (337 nm) at a laser repetition rate of 20 Hz. In both cases, the drift cell was operated at 62 V cm^{-1} Torr^{-1} with helium gas (adapted from Ref. [108]).

instrumentation, and several directions are actively being pursued by a number of groups to enhance the sensitivity and dynamic range obtained in IM–TOFMS instrumentation. For example, advances in pulsed ion funnels [52] and pulsed ion traps [106] as ion transmission and storage devices can significantly improve sensitivity when coupling a continuous ion source such as ESI with IM–MS. Complementary advances are also realized in MALDI–TOFMS by increasing the instrumental duty cycle through the use of high repetition rate laser technology [107]. Recently, moderate energy (10–30 μJ/pulse) high repetition rate (0.5–100 kHz), solid-state, frequency-tripled Nd:YAG and Nd:YLF (355 nm and 349 (or 351) nm, respectively) lasers have become available. Importantly, these lasers exhibit significantly improved primary beam characteristics (e.g., TEM_{00}, Gaussian ~0.25–1 mm diameter ($1/e^2$), divergence ca. 1–4 mrad) over conventional lasers used for MALDI (e.g., cartridge-type nitrogen) while retaining similar temporal attributes (0.5–20 ns versus 4–5 ns pulse widths, respectively). By using high repetition rate (150 Hz) MALDI, sub-fmol absolute detection limits (ca. 0.1 fmol, 3σ) were obtained in the analysis of model peptides by MALDI–IM–TOFMS as illustrated in Fig. 3(C)

[108]. Owing to the improved beam characteristics and higher repetition rate operation, this represents nearly a factor of 60–80 improvement in sample throughput over low repetition rate MALDI operation. Conceptually, two decades of higher sample throughput increases the sample load that can be analyzed from 100 s to >1000 s per day, which is better suited for addressing proteomic-scale experiments where throughput and sensitivity are the central dogma.

1.3. Qualitative and quantitative utility of conformation space in ion mobility–mass spectrometry

One of the primary advantages of conformation space in IM–MS is the separation of molecules of different molecular class as illustrated in Fig. 2(B). Clearly, very high mass measurement accuracy is required to assign the peaks in a mass spectrum to specific classes of compounds based solely on mass spectral data (Fig. 2(B, iii)). For example, there are no mass resolved signals corresponding to polyhistidine ions having S/N ratios greater than 3:1 owing to the large background from chemical noise making identification of the sample constituents impossible by mass spectrometry alone (at this resolution). In addition to the separation of different molecular classes, structural information can be extracted from a detailed analysis of the individual trendlines. The spread of ions in conformation space is much different for biopolymers with non-uniform repeat units (e.g., peptides, oligonucleotides, lipids, etc.), due to variability in both the packing efficiency of different repeat units and gas-phase conformations relative to polymers with regular repeat units [109]. An analysis of a large peptide dataset (>1200 peptides) shows that most peptide ion signals are clustered near the center of a trendline, and the edges of the distribution are sparsely populated (±1–3 and ±10–15% relative standard deviation (RSD), respectively). Although critical measurements have not yet been made, it is likely that molecular classes having greater chemical heterogeneity relative to peptides, e.g., branched carbohydrates, will have comparable or greater spread in conformation space. Peptide signals occurring at the edges of a trendline (i.e., ±10–15% RSD from a best-fit relationship) correspond with: (A) conserved secondary structural motifs, (B) intramolecular solvation of PTMs, and/or (C) small molecule–peptide ligation (Fig. 4). Each of these modifications in gas-phase packing efficiency give rise to increased utilization of conformation space.

For example, α-helices have been extensively studied due to the relative stability of peptide helices compared to other non-close-packed random coil conformations (e.g., β-hairpin) [65]. Most gas-phase peptide ions that are α-helical exhibit a substantially larger collision cross-section than random coil peptides of the same mass (∼10–20% relative difference in ATD) [25,62]. Molecular modeling techniques are typically utilized to obtain detailed structural information for comparison with measured collision cross-sections (Fig. 4(A and B)). Close-packed random coil peptides are predicted to exhibit a relationship between ATD and *m*/*z* that approximates a cube-root function (collision cross-section scales as d^2 (apparent surface area) and mass scales as d^3 (apparent volume)). Thus, packing efficiency for roughly spherically shaped peptide ions increases with increasing *m*/*z*, whereas signals associated with helical peptides are predicted to have a linear relationship removed from that of random coil peptides by as much as 20% in ATD (over the typical tryptic peptide mass range of 500–3000 *m*/*z*). Fig. 4(A) contains data for two peptides LLGNVLVVLAR and LLVVYPWTQR from a tryptic digest of hemoglobin. Although both peptides are nearly of the same mass (1266.61 and 1275.54 Da, respectively), they differ by ca. 5% in experimentally determined collision cross-section. Molecular dynamic simulations suggest that this difference is commensurate with LLGNVLVVLAR exhibiting helical structure versus random coil for LLVVYPWTQR. Note that in most cases, the degree of divergence for helical versus random coil trendlines predicted by theory is not observed, indicating that the conformations observed are not "pure", i.e., that helical trends may contain partial helices and that lower trends may contain random coils that are loosely packed. More detailed experiments, involving chemical modification and extensive molecular dynamics simulations, suggest that the former hypothesis (involving partial helices) is highly probable in most IM–MS measurements [24].

The conformation space of gas-phase peptide ions is also influenced by PTM peptides. For example, phosphorylated peptides and peptides covalently attached to small molecules tend to pack more tightly per unit mass than the majority of unmodified protonated peptide ions (Fig. 4(B) and (C), respectively). Molecular dynamics simulations suggest that in the case of phosphorylation, the peptide solvates the phosphate moiety resulting in a more compact structure than observed for non-phosphorylated peptides (Fig. 4(B), right). These data suggest that IM–MS can be used to perform data-dependent screening for the rapid identification of post-translational modifications in contrast to MS-only approaches where data interpretation can be complicated by neutral loss or the limited or non-existent PTM information in genomic or proteomic databases.

Fig. 4(C) illustrates data for a tryptic digest of horse heart cytochrome *c*. Signals corresponding to heme radical cation (616.18 Da) and heme-containing peptides (i.e., CAQCHTVEK + heme, CAQCHTVEKGGK + heme, IFVQKCAQCHTVEK + heme, KIFVQKCAQCHTVEK + heme) are observed at arrival times substantially shorter than unmodified peptides. Covalent attachment of heme with CAQCHTVEK and peptides arising from missed enzymatic cleavage was confirmed by high-resolution MALDI–TOFMS as illustrated in Fig. 4(C, right) and comparison with the theoretical isotope cluster involving heme [110]. Such results suggest that future developments in IM–MS technology and conformation space analyses could result in a general methodology for the rapid screening of peptide or protein drug interactions that are of keen interest in pharmaceuticals research.

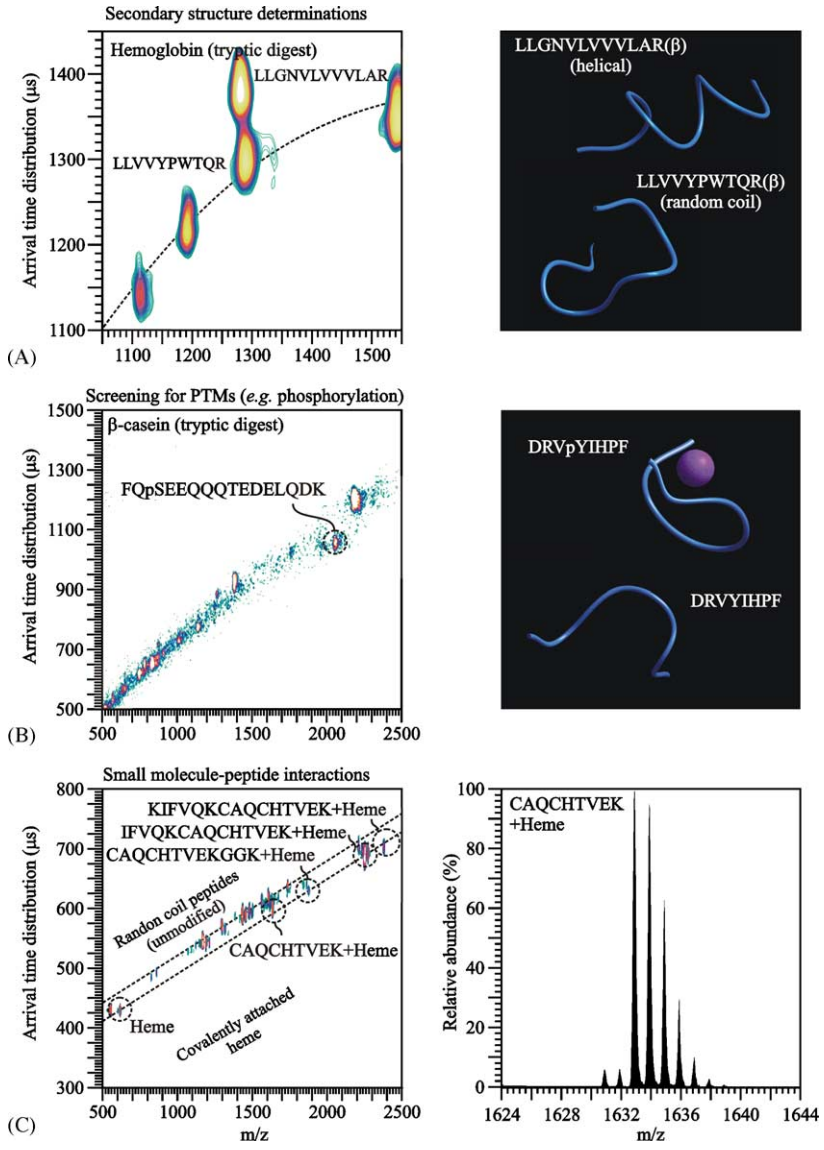

Fig. 4. Two-dimensional IM–MS plots of conformation space illustrating three situations in which conformation space is populated with signals significantly deviating (positively or negatively) from the apparent peptide ATD–*m*/*z* trendline for (A) determination of secondary structure, (B) screening for post-translational modifications, and (C) evaluation of peptide-small molecule interactions. (A) The increase in ATD deviation is indicative of conserved secondary structural elements (e.g., helical, β-hairpin, etc.). (Left): A tryptic digest of bovine hemoglobin where the protonated peptide LLGNVLVVLAR (M_r = 1266.61 Da) exhibits a collision cross-section ca. 5% larger than a protonated peptide of slightly higher mass (LLVVYPWTQR, M_r = 1275.54 Da). (Right): The positive deviation for LLGNVLVVLAR versus LLVVYPWTQR is attributed to conserved helical character in the gas-phase in contrast to typically random coil as determined by molecular dynamics simulations (adapted from Ref. [25]). (B) (left): A proteolytic digest (tryptic) of bovine β-casein where ^{50}Ser is phosphorylated resulting in a negative deviation for the peptide (FQpSEEQQQTEDELQDK, position 48–60 in the protein, MW = 2062.99 Da) as indicated by a dashed line. (B) (right): Molecular dynamics simulation for human angiotensin II with both Tyr phosphorylation (DRVpYIHPF, top) and the non-phosphorylated analog (DRVYIHPF, bottom) illustrating intramolecular solvation of the phosphate group accompanied by a reduction in the collison cross-section (adapted from Ref. [27]). (C) A tryptic digest of horse heart cytochrome *c* as a model for peptide–ligand interactions. The heme porphyrin group ($C_{34}H_{30}O_4N_4Fe$, MW = 616.18 Da) is covalently attached to ^{14}Cys and ^{17}Cys. The three higher mass heme-containing peptides indicated on the lower trendline are proteolytic miscleavage products. In all cases, the identification of heme-containing peptides is confirmed by high-resolution MALDI–TOFMS and inspection of the isotope cluster for Fe as shown in (C, right).

2. Ion mobility for proteomic applications

High-throughput proteomic studies are generally aimed at protein identification based on peptide mass mapping and searching against genomic/proteomic databases [2,111,112]. Initial IM–MS data for peptide mass mapping indicates that a greater number of proteolytically derived peptides are observed by using ion mobility separation prior to mass spectrometry than by MALDI–MS alone [7]. There are several factors that influence the increase in protein sequence cover-

age, and primary among these is the ability of IM–MS to confidently identify low-abundance ion signals in the presence of chemical and/or instrumental noise. By knowing the trendline slope and appearance area for peptide ions in IM–MS conformation space, even peptide ions with a S/N < 3 can be confidently identified and searched against a database for protein identification. Further, there is an apparent decrease in the suppression of Lys-terminated tryptic digest products relative to standard MALDI–TOF analysis, which is attributed to the combination of high-pressure ionization and IM separation prior to sampling in the TOFMS [7]. Hill and coworkers have recently described the utility of using different drift gases to affect the selectivity for peptide ions observed in IM–MS experiments [98]. Complementary to this work, we have observed a larger number of peptide ion signals when using nitrogen or methane as a drift gas as compared to argon or helium separations [40]. In addition, combining the peptide signals observed in different drift gases significantly enhances protein sequence coverage over conventional MALDI–TOFMS alone [113]. The mechanisms for the apparent change in the number of observable peptide ion signals as a function of drift gas are still unclear and are a topic of active research.

In parallel with peptide mass-mapping techniques, tandem mass spectrometry (MS/MS) technology has become an indispensable tool for proteome analysis by providing sequence tags for higher-confidence level protein identification than are capable by only peptide mass-mapping strategies [112]. In most cases, MS/MS technology is operated in a scanning mode, i.e., a mass filter is set to transmit a particular mass (or range of masses), the selected ions are activated (e.g., by collision-induced dissociation (CID)) and fragment via unimolecular decay processes to produce sequence-informative fragment ions, which are subsequently analyzed by a second mass spectrometer. This approach, while effective for a continuous source of ions, is typically less efficient for a time-varying ion population, e.g., the output of a chromatographic separation, unless a means for stopping the separation, i.e., "peak parking" is used [114,115]. This scanning configuration is also undesirable from a high-throughput standpoint, as each iterative scan takes additional time to accomplish. The ideal tandem mass spectrometer would allow for the simultaneous acquisition of parent ions and fragment ions with spatial or temporal correlation, to retain information content, e.g., that derived in the separation dimension [116]. Recently, IM–MS/MS separations utilizing an ion activation region after the IM drift cell (e.g., by CID [48], surface induced dissociation (SID) [8,47], or photodissociation [49]) followed by mass analysis have been demonstrated as a method for providing a series of temporally correlated and parallel tandem mass spectrometry experiments. The IM–MS/MS experiment is capable of providing several tandem mass spectra in addition to the complete peptide mass map in a single experiment, thus providing advantages in terms of throughput, sample consumption, and instrumental duty cycle over scanning tandem mass spectrometry.

Although the ability to perform multiple tandem mass spectrometry experiments in parallel is the primary advantage of IM–MS/MS methods, there are other advantageous aspects of IM–MS/MS that are pertinent to peptide sequencing. Fig. 5(B) shows a typical MALDI–IM–MS/MS experiment utilizing SID for a mixture of the two tryptic peptides shown in Fig. 4(A) (LLGNVLVVVLAR and LLVVYPWTQR). Note the temporal correlation of fragment ions (horizontal trends in the data) with respect to the parent ions (Fig. 5(B, iii and iv)). The individual fragment ion spectra for each peptide can be acquired by integrating across the ATD profile for each peptide (from 1450 to 1525 μs and 1375 to 1440 μs for (iii) and (iv), respectively). In this example, the two tryptic peptides are separated by ∼9 Da, a mass difference that is difficult to resolve using available timed-ion selection with state-of-the-art TOF–TOF instrumentation [117], where the mass window for typical proteolytically derived peptides is ca. 10 Da. Conversely, these two peptides can be easily separated and fragmented to obtain sequence informative fragment ion information using IM–MS/MS due to differences in gas-phase conformation where $[LLGNVLVVVLAR + H]^+$ is partially helical and $[LLVYPWTQR + H]^+$ is random coil in the gas-phase (see Fig. 4(A)); this results in a ∼10% difference between the two signals in IM drift time [24,25]. Note that in conformation space, fragmentation data can also be acquired for multiple conformational forms of the same analyte using IM–MS/MS, which is not possible by conventional tandem mass spectrometry approaches [29,118].

Although a variety of means for post-IM ion activation can be used, there are several advantages to activating the ions via a collision with a surface rather than multiple collisions with inert gas molecules [47]. For example, SID provides (i) a narrow velocity distribution of post-dissociation fragment ions [119], (ii) a relatively high abundance of amino acid side-chain cleavage products to unambiguously assign peptide ion isobars (e.g., Ile versus Leu) similar to high-energy CID [120] or single photon photodissociation [49,121,122], (iii) relatively short dissociation times (<10 μs) owing to unimolecular decay, and (iv) instrumental simplicity. Reported limitations of SID include a propensity to form low mass and non sequence-informative fragment ions and generally low mass resolution for SID fragment ion spectra [119]. However, the sequencing data shown in Fig. 5(B, iii and iv) are sufficient to unambiguously identify both parent species. In general, a relatively high abundance of high-mass sequence-informative fragment ions using IM–MS/MS with SID-activated peptides is observed [47]. This IM–SID–MS/MS configuration utilized a linear TOFMS that allowed SID fragments with a wide kinetic energy distribution to be sampled in the direction of the TOF analyzer [47]. A second generation "*Z*-configuration" IM–SID–MS/MS instrument was recently constructed (Fig. 5(A)) and can routinely provide higher peptide mass resolution (∼4000) by positioning the surface 45° relative to the orthogonal extraction source of a reflectron TOF and in-line with the primary ion beam [123].

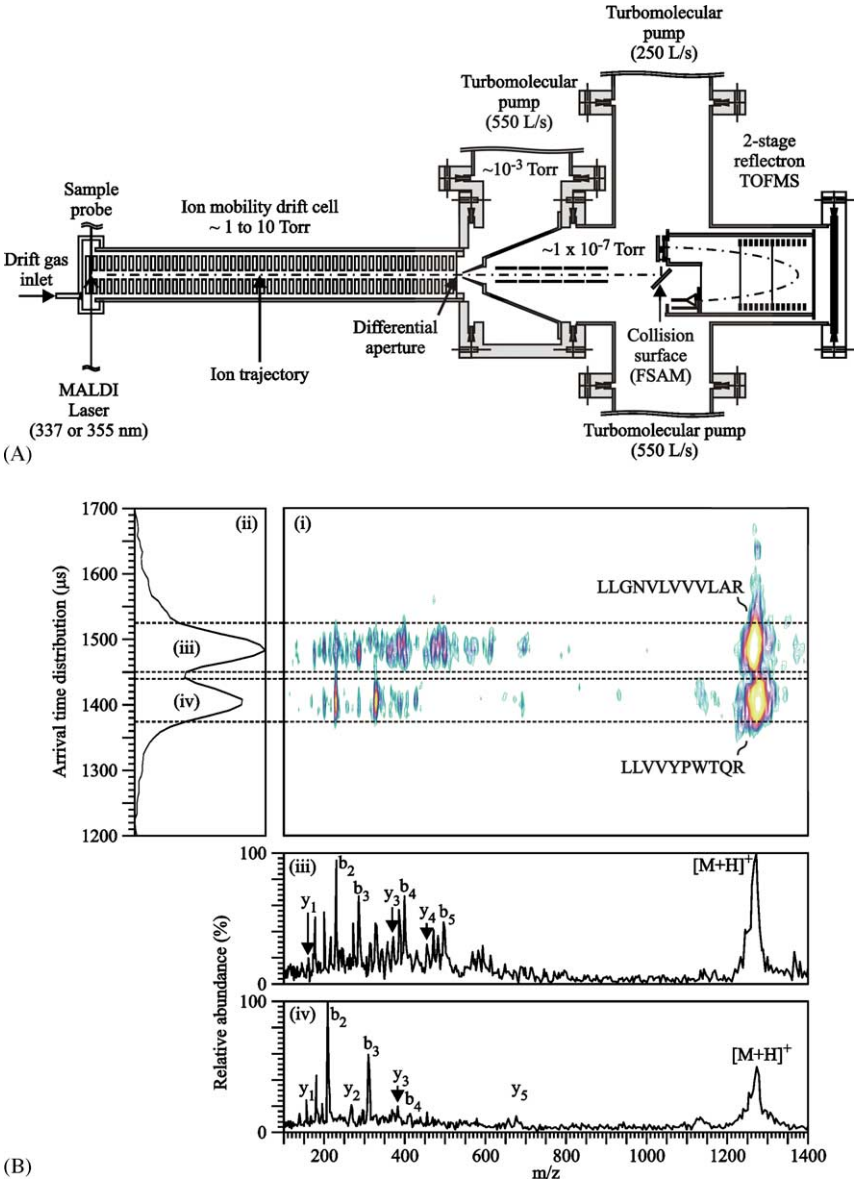

Fig. 5. (A) Schematic diagram of the third-generation MALDI–IM–SID–TOFMS arrangement used in our laboratories for IM–MS/MS determinations. (B): (i) Two-dimensional IM–MS/MS plot of conformation space showing the separation of precursor and corresponding fragment ion spectra of two peptides from bovine hemoglobin (LLGNVLVVVLAR and LLVVTPWTQR, respectively, designated as helical (i) and random coil (ii) in Fig. 4A). (ii) The ion mobility ATD integrated over all *m*/*z* space. (iii) and (iv) The integrated mass spectra over ATD space corresponding to the correlated fragment ions from these two peptides (1375–1440 μs (iv) and 1450–1525 μs (iii), regions outlined by dashed-lines) are shown with several abundant *y*- and *b*-type fragment ions labeled.

3. The new paradigm for proteomics: emerging avenues for IM–MS

This report illustrates several examples of the unique attributes inherent in coupling IM–MS or IM–MS/MS with proteomic applications, for example: (i) rapid 2D separations (μs–ms) in comparison with LC or CE–MS (min–h), (ii) reduction of chemical noise and ion suppression effects, (iii) fast separation of molecules of different molecular and/or conformational class, and (iv) nearly simultaneous acquisition of both parent and fragment ion spectra. Although IM–MS is not a routine technique for proteomic studies, this situation will likely change as commercial instrumentation becomes available. Our group and others are developing instrumentation to overcome several of the challenges that exist with contemporary instrumental designs. For proteomic applications, the specific challenge with IM–MS instrumentation is sensitivity and consequently throughput. In the sections above, several means are described to assist in alleviating this limitation.

We began development of MALDI–IM–TOFMS [89] after several years of experience in developing high-resolution

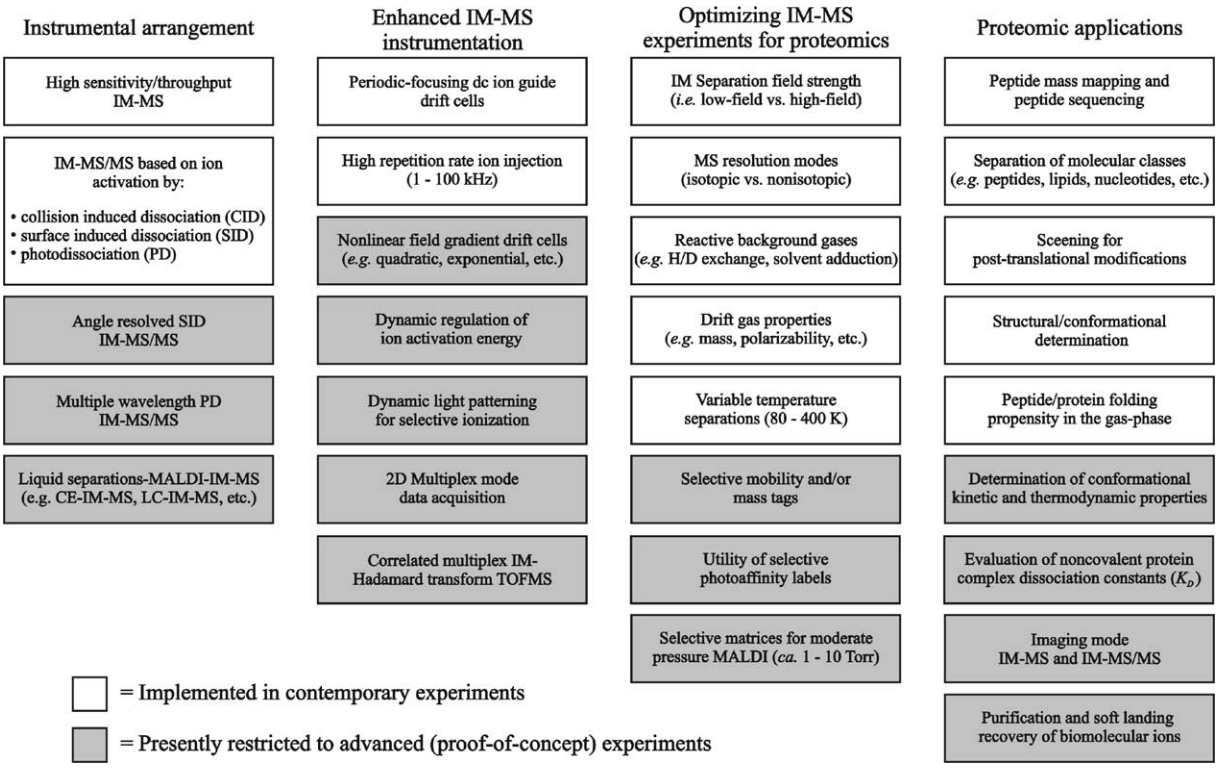

Fig. 6. Chart illustrating present and future IM–MS instrument and proteomic applications development efforts in our laboratory and collaborating institutions.

TOFMS instrumentation [12,124]; this venture was motivated by the desire to transform data into information and biochemical understanding. Specific innovations developed in our laboratory and with our collaborators are shown in Fig. 6. These advances are generally classified by (i) different experimental arrangements, (ii) methodology for enhancing the figures of merit for existing configurations, (iii) techniques for optimizing the IM–MS experiment, and (iv) the types of information that can be acquired for proteomic studies. The specific motivation for these advances is to better facilitate the rapid dissemination of proteomic data to resolve questions at the forefront of chemical biology. In this vein, instrumental advances are aimed at providing higher sensitivity, faster analysis times, higher information content, and tunable selectivity. Analogous to contemporary advances in TOFMS, both sensitivity and dynamic range can be significantly improved in IM–TOFMS by using multiplex data-acquisition methods [125,126] and position-sensitive detection strategies [105]. By multiplexing ion injection into the drift cell (MALDI or ESI), throughput can be enhanced by factors of 10^2 to 10^4 and combined with multiplexed TOFMS [127,128] these factors can be increased further to 10^3 to 10^6. By utilizing position sensitive detection with IM–TOFMS, dynamic range can be improved from ca. 10^4 to 10^5 to potentially greater than seven decades. Furthermore, advances in MALDI are directly transferable to MALDI–IM–TOFMS instrumentation (see for example, Refs. [129–133]).

Caprioli and colleagues first described MALDI imaging MS for the direct imaging of peptides and proteins in thin (ca. 15 μm) tissue sections [129]. The practical implementation of MALDI imaging-mode MS is illustrated in Fig. 7, whereby the MALDI laser is rastered with respect to the sample in a spatially resolved manner and particular *m*/*z* ions are subsequently interrogated in a matrix format (Fig. 7(A)). However, the challenges associated with characterizing analytes of interest become more difficult as the complexity of the sample increases. In particular, the spectra can be further congested due to peak overlap by concomitant species of different molecular class (derived from e.g., salts, detergents, tissue fixing agents, lipids, oligonucleotides, glycoconjugates, etc.). Several of these challenges can be overcome by performing post-ionization IM–MS and separating the analytes in conformation space (Fig. 7(B)). A further challenge in imaging-mode MS experiments is the difficulty in performing scanning MS/MS analyses for complementary sequence tag information. This arises because of the limited amount of sample at each spatial position. By using imaging-mode IM–MS/MS, virtually all of the analytes present can be activated prior to mass analysis (rather than scanning), which provides a Fellgett advantage that is well suited to the analysis of limited samples. New dynamic light patterning for MALDI–MS imaging applications will also advance the speed and spatial resolution available in imaging-mode applications, which are readily interfaced to IM–MS and IM–MS/MS instrumentation [134,135]. Further advances in imaging-mode operation can be obtained by innovations in both, IM or MS dimensions.

Enhancing separations based on changing the IM conditions such as using reactive background gases [136,137],

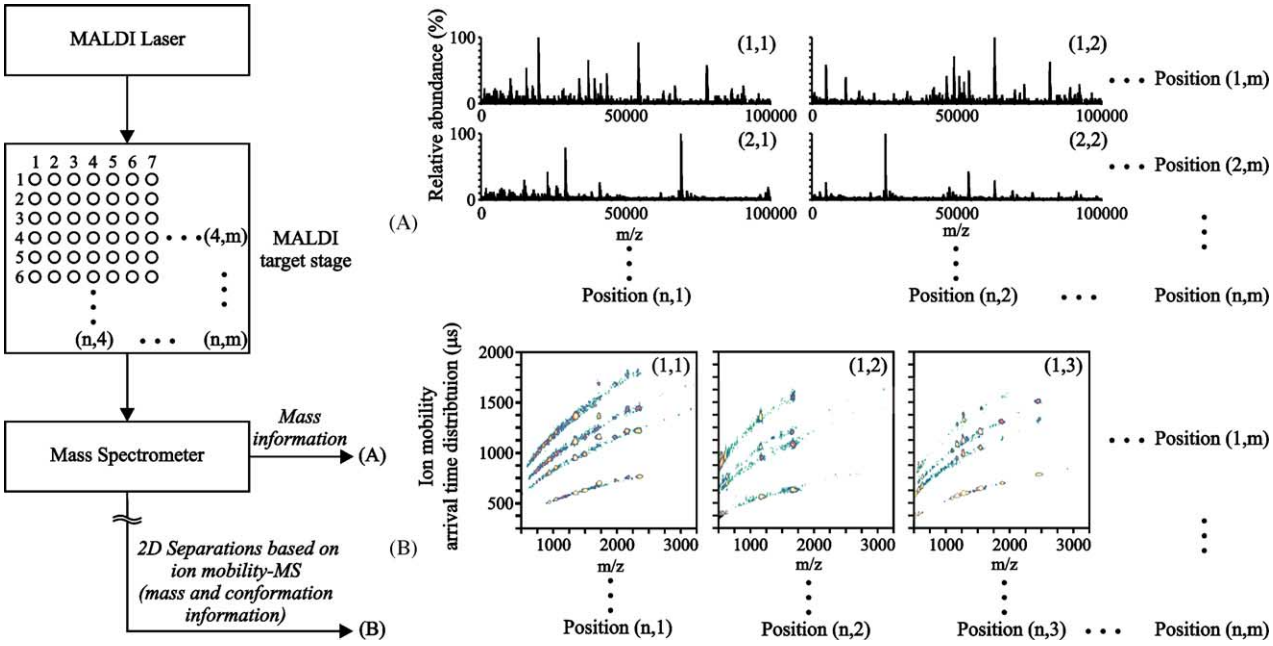

Fig. 7. (Left): a conceptual flowchart of contemporary imaging MS. (A) The molecular information gained in a conventional imaging MS experiment in a spatially-resolved manner. (B) Two-dimensional molecular information obtained in conformation space utilizing imaging IM–MS in a matrix format.

mixed gases [40,98], non-linear electric field gradients [103], and altering electric field strengths [54,138], provides a relatively non-intrusive means for altering selectivity, separation time, and ion transmission efficiency. Alternatively, selective chemical methods for changing the ultimate collision cross-section by using mobility tags, photoaffinity labeling [139], or addition of an affinity mass tag can provide an additional means for selectively identifying biomolecules exhibiting a particular function or conformation. This is in contrast to MS-only methods, which are typically only sensitive to changes in mass (e.g., isotope tagging or isotope-coded affinity tagging [140]) unless additional means are used to first isolate and subsequently probe the reacted products (at the consequence of analysis time). Importantly, each of these methods for optimizing IM separation conditions is commensurate with IM–MS/MS methodologies and the use of alternative ion activation techniques such as photodissociation [49] and angle-resolved SID [123].

Parallel to new techniques for proteomic applications, ion mobility also provides a unique means for probing the biophysical attributes of gas-phase ion structures and conformations. Variable temperature IM can provide kinetic and thermodynamic insight into gas-phase protein folding and unfolding processes [50–53]. Moreover, IM–MS provides a well-controlled environment for investigating solvation effects by allowing the stepwise addition of solvent [67]. Furthermore, IM–MS provides a unique means of determining dissociation constants of non-covalent protein complexes, which is of considerable utility in functional and structural biology. The new paradigm in proteomic research is the development of methodology to derive biochemical information and understanding in addition to conventional protein identification. In IM–MS, this is afforded by structural dimensionality in conformation space and an ability to perform parallel correlated experiments with limited samples. In tandem with instrumental advances, IM methodology will certainly play a significant role in the modern proteomics laboratory and offers new horizons for addressing proteomic and biophysical questions.

Acknowledgements

Financial support for this work was provided by the National Institutes of Health (1R01 RR01958701), the National Science Foundation (MRI-0116685), the Department of Energy Division of Chemical Sciences, BES (DE-FG03-95ER14505), the Texas Advance Research Program/ Advanced Technology Program (TARP/TDT, 010366-0064-2001), and Ionwerks Inc.

References

[1] R. Aebersold, M. Mann, Nature 422 (2003) 198.
[2] W.J. Henzel, C. Watanabe, J.T. Stults, J. Am. Soc. Mass Spectrom. 14 (2003) 931.
[3] E.K. Fridriksson, A. Beavil, D. Holowka, H.J. Gould, B. Baird, F.W. McLafferty, Biochemistry 39 (2000) 3369.
[4] W. Mo, B.L. Karger, Curr. Opin. Chem. Biol. 6 (2002) 666.
[5] Ph. Dugourd, R.R. Hudgins, D.E. Clemmer, M.F. Jarrold, Rev. Sci. Inst. 68 (1997) 1122.
[6] C. Wu, W.F. Siems, G.R. Asbury, H.H. Hill Jr., Anal. Chem. 70 (1998) 4929.
[7] B.T. Ruotolo, K.J. Gillig, E.G. Stone, D.H. Russell, K. Fuhrer, M. Gonin, J.A. Schultz, Int. J. Mass Spectrom. 219 (2002) 253.

[8] E. Stone, K.J. Gillig, B. Ruotolo, K. Fuhrer, M. Gonin, A. Schultz, D.H. Russell, Anal. Chem. 73 (2001) 2233.
[9] C. O'Donovan, R. Apweiler, A. Bairoch, Trends Biotechnol. 19 (2001) 178.
[10] R.F. Service, Science 302 (2003) 1316.
[11] B.P.Y. Lau, D. Weber, J.J. Ryan, Instrum. Trace Org. Monit. (1992) 155.
[12] R.D. Edmondson, D.H. Russell, J. Am. Soc. Mass Spectrom. 7 (1996) 995.
[13] R. Bischoff, Anal. Bioanal. Chem. 376 (2003) 289.
[14] T. Manabe, J. Chromatogr. B 787 (2003) 29.
[15] H. Wang, S. Hanash, J. Chromatogr. B 787 (2003) 11.
[16] J.F. Holland, C.G. Enke, J. Allison, J.T. Stults, J.D. Pinkston, B. Newcome, J.T. Watson, Anal. Chem. 55 (1983) 997A.
[17] A.J. Link, J. Eng, D.M. Schieltz, E. Carmack, G.J. Mize, D.R. Morris, B.M. Garvik, J.R. Yates III, Nat. Biotech. 17 (1999) 676.
[18] D.A. Wolters, M.P. Washburn, J.R. Yates III, Anal. Chem. 73 (2001) 5683.
[19] E.F. Strittmatter, P.L. Ferguson, K. Tang, R.D. Smith, J. Am. Soc. Mass Spectrom. 14 (2003) 980.
[20] G.F. Verbeck, K.J. Gillig, D.H. Russell, Eur. J. Mass Spectrom. 9 (2003) 579.
[21] M. Karas, Separation of Components of an Analysis Sample in an Ion Mobility Spectrometer Using a Supply of Selectively Interactive Gaseous Particles, (Int. patent #WO02096805, December 5, 2002).
[22] A.E. Counterman, D.E. Clemmer, Anal. Chem. 74 (2002) 1946.
[23] R.R. Hudgins, M.A. Ratner, M.F. Jarrold, J. Am. Chem. Soc. 120 (1998) 12974.
[24] B.T. Ruotolo, D.H. Russell, J. Phys. Chem. B 108 (2004) 15321.
[25] B.T. Ruotolo, G.F. Verbeck, L.M. Thomson, K.J. Gillig, D.H. Russell, J. Am. Chem. Soc. 124 (2002) 4214.
[26] T. Wyttenbach, G. von Helden, M.T. Bowers, J. Am. Chem. Soc. 118 (1996) 8355.
[27] B.T. Ruotolo, G.F. Verbeck, L.M. Thomson, A.S. Woods, K.J. Gillig, D.H. Russell, J. Proteome Res. 1 (2002) 303.
[28] B.T. Ruotolo, C.C. Tate, D.H. Russell, J. Am. Soc. Mass Spectrom. 15 (2004) 870.
[29] H.A. Sawyer, J.T. Marini, B.T. Ruotolo, K.J. Gillig, D.H. Russell, J. Am. Soc. Mass Spectrom. (2004) submitted for publication.
[30] A.S. Woods, J.M. Koomen, B.T. Ruotolo, K.J. Gillig, D.H. Russell, K. Fuhrer, M. Gonin, T.F. Egan, J.A. Schultz, J. Am. Soc. Mass Spectrom. 13 (2002) 166.
[31] D.T. Kaleta, M.F. Jarrold, J. Phys. Chem. A 106 (2002) 9655.
[32] D.T. Kaleta, M.F. Jarrold, J. Phys. Chem. B 107 (2003) 14529.
[33] D. Liu, T. Wyttenbach, C.J. Carpenter, M.T. Bowers, J. Am. Chem. Soc. 126 (2004) 3261.
[34] Y. Shen, R. Zhao, M.E. Belov, T.P. Conrads, G.A. Anderson, K. Tang, L. Pasa-Tolic, T.D. Veenstra, M.S. Lipton, H.R. Udseth, R.D. Smith, Anal. Chem. 73 (2001) 1766.
[35] J.E. MacNair, K.D. Patel, J.W. Jorgenson, Anal. Chem. 71 (1999) 700.
[36] A. Grall, C. Leonard, R. Sacks, Anal. Chem. 72 (2000) 591.
[37] J.M. Hille, A.L. Freed, H. Watzig, Electrophoresis 22 (2001) 4035.
[38] A.W. Moore Jr., J.W. Jorgenson, Anal. Chem. 67 (1995) 3448.
[39] Y. Shen, N. Tolic, R. Zhao, L. Pasa-Tolic, L. Li, S.J. Berger, R. Harkewicz, G.A. Anderson, M.E. Belov, R.D. Smith, Anal. Chem. 73 (2001) 3011.
[40] B.T. Ruotolo, J.A. McLean, K.J. Gillig, D.H. Russell, J. Mass Spectrom. 39 (2004) 361.
[41] S.J. Valentine, M. Kulchania, C.A. Srebalus Barnes, D.E. Clemmer, Int. J. Mass Spectrom. 212 (2001) 97.
[42] A.W. Moore Jr., J.W. Jorgenson, Anal. Chem. 67 (1995) 3456.
[43] J.C. Giddings, Anal. Chem. 56 (1984) 1258A.
[44] J.M. Koomen, B.T. Ruotolo, K.J. Gillig, J.A. McLean, D.H. Russell, M. Kang, K.R. Dunbar, K. Fuhrer, M. Gonin, J.A. Schultz, Anal. Bioanal. Chem. 373 (2002) 612.
[45] A.S. Woods, M. Ugarov, T. Egan, J. Koomen, K.J. Gillig, K. Fuhrer, M. Gonin, J.A. Schultz, Anal. Chem. 76 (2004) 2187.
[46] B.T. Ruotolo, K.J. Gillig, D.H. Russell, J. Proteome Res. (2004) submitted for publication.
[47] E.G. Stone, K.J. Gillig, B.T. Ruotolo, D.H. Russell, Int. J. Mass Spectrom. 212 (2001) 519.
[48] C.S. Hoaglund-Hyzer, J. Li, D.E. Clemmer, Anal. Chem. 72 (2000) 2737.
[49] J.A. McLean, K.J. Gillig, B.T. Ruotolo, M. Ugarov, H. Bensaoula, T. Egan, J.A. Schultz, D.H. Russell, Proceedings of the 51st Conference of the American Society for Mass Spectrometry, Montreal, Canada, 2003.
[50] T. Wyttenbach, M.T. Bowers, Top. Curr. Chem. 225 (2003) 207.
[51] P.R. Kemper, M.T. Bowers, J. Am. Soc. Mass Spectrom. 1 (1990) 197.
[52] T. Wyttenbach, P.R. Kemper, M.T. Bowers, Int. J. Mass Spectrom. 212 (2001) 13.
[53] B.S. Kinnear, M.R. Hartings, M.F. Jarrold, J. Am. Chem. Soc. 123 (2001) 5660.
[54] G.F. Verbeck, B.T. Ruotolo, K.J. Gillig, D.H. Russell, J. Am. Soc. Mass Spectrom. 15 (2004) 1320.
[55] M.F. Jarrold, Annu. Rev. Phys. Chem. 51 (2000) 179.
[56] T. Wyttenbach, E.S. Baker, S.L. Bernstein, A. Ferzoco, J. Gidden, D. Liu, M.T. Bowers, in: A.E. Ashcroft, G. Breton, J.J. Monaghan (Eds.), Advances in Mass Spectrometry, vol. 16, Elsevier, Amsterdam, 2004, p. 189, Chapter 11.
[57] S.L. Bernstein, D. Liu, T. Wyttenbach, M.T. Bowers, J.C. Lee, H.B. Gray, J.R. Winkler, J. Am. Soc. Mass Spectrom. 15 (2004) 1435.
[58] T. Ideker, T. Galitski, L. Hood, Annu. Rev. Genom. Hum. Gen. 2 (2001) 343.
[59] G. von Helden, T. Wyttenbach, M.T. Bowers, Science 267 (1995) 1483.
[60] R.R. Hudgins, M.F. Jarrold, J. Am. Chem. Soc. 121 (1999) 3494.
[61] D.T. Kaleta, M.F. Jarrold, J. Phys. Chem. B 105 (2001) 4436.
[62] B.S. Kinnear, M.R. Hartings, M.F. Jarrold, J. Am. Chem. Soc. 124 (2002) 4422.
[63] D.T. Kaleta, M.F. Jarrold, J. Am. Chem. Soc. 124 (2002) 1154.
[64] D.T. Kaleta, M.F. Jarrold, J. Am. Chem. Soc. 125 (2003) 7186.
[65] G.A. Breaux, M.F. Jarrold, J. Am. Chem. Soc. 125 (2003) 10740.
[66] R. Sudha, M. Kohtani, G.A. Breaux, M.F. Jarrold, J. Am. Chem. Soc. 126 (2004) 2777.
[67] J. Woenckhaus, Y. Mao, M.F. Jarrold, J. Phys. Chem. B 101 (1997) 847.
[68] J. Woenckhaus, R.R. Hudgins, M.F. Jarrold, J. Am. Chem. Soc. 119 (1997) 9586.
[69] J.L. Fye, J. Woenckhaus, M.F. Jarrold, J. Am. Chem. Soc. 120 (1998) 1327.
[70] M.F. Jarrold, Acc. Chem. Res. 32 (1999) 360.
[71] Y. Mao, M.A. Ratner, M.F. Jarrold, J. Am. Chem. Soc. 122 (2000) 2950.
[72] M. Kohtani, M.F. Jarrold, J. Am. Chem. Soc. 124 (2002) 11148.
[73] M. Kohtani, G.A. Breaux, M.F. Jarrold, J. Am. Chem. Soc. 126 (2004) 1206.
[74] D.E. Clemmer, R.R. Hudgins, M.F. Jarrold, J. Am. Chem. Soc. 117 (1995) 10141.
[75] K.B. Shelimov, M.F. Jarrold, J. Am. Chem. Soc. 118 (1996) 10313.
[76] K.B. Shelimov, D.E. Clemmer, R.R. Hudgins, M.F. Jarrold, J. Am. Chem. Soc. 119 (1997) 2240.
[77] S.J. Valentine, D.E. Clemmer, J. Am. Chem. Soc. 119 (1997) 3558.
[78] S.J. Valentine, J. Anderson, A.E. Ellington, D.E. Clemmer, J. Phys. Chem. B 101 (1997) 3891.
[79] E.R. Badman, C.S. Hoaglund-Hyzer, D.E. Clemmer, Anal. Chem. 73 (2001) 6000.
[80] S. Myung, E. Badman, Y.J. Lee, D.E. Clemmer, J. Phys. Chem. A 106 (2002) 9976.
[81] S.B. Prusiner, Annu. Rev. Med. 38 (1987) 381.
[82] S.B. Prusiner, M.R. Scott, Annu. Rev. Genet. 31 (1997) 139.

[83] J. Collinge, Annu. Rev. Neurosci. 24 (2001) 519.
[84] C.J. Barrow, M.G. Zagorski, Science 253 (1991) 179.
[85] K. Tanaka, H. Waki, Y. Ido, S. Akita, Y. Yoshida, T. Yohida, Rapid Commun. Mass Spectrom. 2 (1988) 151.
[86] M. Karas, F. Hillenkamp, Anal. Chem. 60 (1988) 2299.
[87] J.B. Fenn, M. Mann, C.K. Meng, S.F. Wong, C.M. Whitehouse, Science 246 (1989) 64.
[88] G. von Helden, T. Wyttenbach, M.T. Bowers, Int. J. Mass Spectrom. Ion Proc. 146–147 (1995) 349.
[89] K.J. Gillig, B.T. Ruotolo, E.G. Stone, D.H. Russell, K. Fuhrer, M. Gonin, J.A. Schultz, Anal. Chem. 72 (2000) 3965.
[90] W.E. Steiner, B.H. Clowers, W.A. English, H.H. Hill Jr., Rap. Commun. Mass Spectrom. 18 (2004) 882.
[91] G. von Helden, M.-T. Hsu, P.R. Kemper, M.T. Bowers, J. Chem. Phys. 95 (1991) 3835.
[92] D.E. Clemmer, M.F. Jarrold, J. Mass Spectrom. 32 (1997) 577.
[93] E.A. Mason, E.W. McDaniel, Transport Properties of Ions in Gases, John Wiley and Sons, New York, 1988, p. 31, Chapter 2.
[94] C.B. Shumate, H.H. Hill Jr., Anal. Chem. 61 (1989) 601.
[95] C.S. Hoaglund-Hyzer, Y.J. Lee, A.E. Counterman, D.E. Clemmer, Anal. Chem. 74 (2002) 992.
[96] S. Rokushika, H. Hatano, M.A. Baim, H.H. Hill Jr., Anal. Chem. 57 (1985) 1902.
[97] P. Watts, A. Wilder, Int. J. Mass Spectrom. Ion Proc. 112 (1992) 179.
[98] G.R. Ashbury, H.H. Hill Jr., Anal. Chem. 72 (2000) 580.
[99] C.E. Berry, Rev. Sci. Instrum. 27 (1956) 849.
[100] A. Graber, P.S. Juhasz, N. Khainovski, K.C. Parker, D.H. Patterson, S.A. Martin, Proteomics 4 (2004) 474.
[101] J.A. Loo, Int. J. Mass Spectrom. 200 (2000) 175.
[102] R.L. Winston, M.C. Fitzgerald, Mass Spectrom. Rev. 16 (1997) 165.
[103] K.J. Gillig, B.T. Ruotolo, E.G. Stone, D.H. Russell, Int. J. Mass Spectrom. 239 (2004) 43.
[104] R.J. Cotter, Time-of-Flight Mass Spectrometry: Instrumentation and Applications in Biological Research, American Chemical Society, Washington, DC, 1997.
[105] K. Fuhrer, M. Gonin, M.I. McCully, T. Egan, S.R. Ulrich, V.W. Vaughn, W.D. Burton, J.A. Schultz, K. Gillig, D.H. Russell, Proceedings of the 49th Conference of the American Society for Mass Spectrometry, Chicago, IL, 2001.
[106] C.S. Hoaglund, S.J. Valentine, D.E. Clemmer, Anal. Chem. 69 (1997) 4156.
[107] J.A. McLean, W.K. Russell, D.H. Russell, Anal. Chem. 75 (2003) 648.
[108] J.A. McLean, D.H. Russell, J. Proteome Res. 2 (2003) 427.
[109] B.T. Ruotolo, K.J. Gillig, E.G. Stone, D.H. Russell, J. Chromatogr. B 782 (2002) 385.
[110] D.H. Russell, R.D. Edmondson, J. Mass Spectrom. 32 (1997) 263.
[111] W.J. Henzel, T.M. Billeci, J.T. Stults, S.C. Wong, C. Grimley, C. Watanabe, Proc. Natl. Acad. Sci. U.S.A. 90 (1993) 5011.
[112] J.R. Yates III, Electrophoresis 19 (1998) 893.
[113] J.A. McLean, B.T. Ruotolo, K.J. Gillig, D.H. Russell, Proceedings of the 2002 Lost Pines Molecular Biology Conference, Smithville, TX, 2002.
[114] R.E. Moore, L. Licklider, D. Schumann, T.D. Lee, Anal. Chem. 70 (1998) 4879.
[115] B. Gallis, G.L. Corthals, D.R. Goodlett, H. Ueba, F. Kim, S.R. Presnell, D. Figeys, D.G. Harrison, B.C. Berk, R. Aebersold, M.A. Corson, J. Bio. Chem. (1999) 30101.
[116] F.W. McLafferty (Ed.), Tandem Mass Spectrometry, Plenum Press, New York, 1983.
[117] K.F. Medzihradszky, J.F. Campbell, M.A. Baldwin, A.M. Falick, P. Juhasz, M.L. Vestal, A.L. Burlingame, Anal. Chem. 72 (2000) 552.
[118] E.R. Badman, C.S. Hoaglund-Hyzer, D.E. Clemmer, J. Am. Soc. Mass Spectrom. 13 (2002) 719.
[119] V. Grill, J. Shen, C. Evans, R.G. Cooks, Rev. Sci. Inst. 72 (2001) 3149.
[120] R.S. Johnson, S.A. Martin, K. Biemann, Int. J. Mass Spectrom. Ion Proc. 86 (1988) 137.
[121] M.E. Gimon-Kinsel, G.R. Kinsel, R.D. Edmondson, D.H. Russell, J. Am. Soc. Mass Spectrom. 6 (1995) 578.
[122] D.C. Barbacci, D.H. Russell, J. Am. Soc. Mass Spectrom. 10 (1999) 1038.
[123] W. Sun, K.J. Gillig, D.H. Russell, Proceedings of the 52nd Conference of the American Society for Mass Spectrometry, Nashville, TN, 2004.
[124] D.C. Barbacci, R.D. Edmonson, D.H. Russell, Int. J. Mass Spectrom. 165–166 (1997) 221.
[125] J.A. McLean, D.H. Russell, T.F. Egan, M.V. Ugarov, J.A. Schultz, Multiplex Data Acquisition Modes for Ion Mobility–Mass Spectrometry (US Prov. Patent Filed July 27, 2004).
[126] J.A. McLean, D.H. Russell, Int. J. Ion Mobility Spectrom. (2004) in press.
[127] F.J. Knorr, M. Ajami, D.A. Chatfield, Anal. Chem. 58 (1986) 690.
[128] A. Brock, N. Rodriguez, R.N. Zare, Anal. Chem. 70 (1998) 3735.
[129] R.M. Caprioli, T.B. Farmer, J. Gile, Anal. Chem. 69 (1997) 4751.
[130] M. Traini, A.A. Gooley, K. Ou, M.R. Wilkins, L. Tonella, J.-C. Sanchez, D.F. Hochstrasser, K.L. Williams, Electrophoresis 19 (1998) 1941.
[131] J. Wei, J.M. Buriak, G. Siuzdak, Nature 399 (1999) 243.
[132] V.V. Laiko, M.A. Baldwin, A.L. Burlingame, Anal. Chem. 72 (2000) 652.
[133] A. Novikov, M. Caroff, S. Della-Negra, Y. Lebeyec, M. Pautrat, J.A. Schultz, A. Tempez, H.-W.J. Wang, S.N. Jackson, A.S. Woods, Anal. Chem. (2004) in press.
[134] J.A. McLean, D.H. Russell, Advanced Optics for Rapidly Patterned Laser Profiles in Analytical Mass Spectrometry (US Prov. Patent filed February 12, 2004).
[135] S.D. Sherrod, J.A. McLean, D.H. Russell, Proceedings of the 52nd Conference of the American Society for Mass Spectrometry, Nashville, TN, 2004.
[136] G.W. Griffin, I. Dzidic, D.I. Carroll, R.N. Stillwell, E.C. Horning, Anal. Chem. 45 (1973) 1204.
[137] D.I. Carroll, I. Dzidic, R.N. Stillwell, E.C. Horning, Anal. Chem. 47 (1975) 1956.
[138] B.T. Ruotolo, J.A. McLean, K.J. Gillig, D.H. Russell, J. Am. Soc. Mass Spectrom., 2004, submitted for publication.
[139] R.E. Bossio, R.R. Hudgins, A.G. Marshall, J. Phys. Chem. B 107 (2003) 3284.
[140] S.P. Gygi, B. Rist, S.A. Gerber, F. Turecek, M.H. Gelb, R. Aebersold, Nat. Biotech. 17 (1999) 994.